TISSUE ENGINEERING: Part A
Volume 25, Numbers 11 and 12, 2019
Mary Ann Liebert, Inc.
DOI: 10.1089/ten.tea.2018.0067

termis
Tissue Engineering
& Regenerative Medicine
International Society

ORIGINAL ARTICLE

Generation of Functional Human Adipose Tissue in Mice from Primed Progenitor Cells

Raziel Rojas-Rodriguez,[1,*] Jorge Lujan-Hernandez, MD,[2,*] So Yun Min, PhD,[1,*] Tiffany DeSouza,[1,*] Patrick Teebagy,[2] Anand Desai, MS,[1] Heather Tessier,[2] Robert Slamin,[2] Leah Siegel-Reamer,[2] Cara Berg,[1] Angel Baez,[2] Janice Lalikos, MD,[2,†] and Silvia Corvera, MD[1,†]

Adipose tissue (AT) is used extensively in reconstructive and regenerative therapies, but transplanted fat often undergoes cell death, leading to inflammation, calcification, and requirement for further revision surgery. Previously, we have found that mesenchymal progenitor cells within human AT can proliferate in three-dimensional culture under proangiogenic conditions. These cells (primed ADipose progenitor cells, PADS) robustly differentiate into adipocytes *in vitro* (ad-PADS). The goal of this study is to determine whether ad-PADS can form structured AT *in vivo*, with potential for use in surgical applications. Grafts formed from ad-PADS were compared to grafts formed from AT obtained by liposuction after implantation into nude mice. Graft volume was measured by microcomputed tomography scanning, and the functionality of cells within the graft was assessed by quantifying circulating human adiponectin. The degree of graft vascularization by donor or host vessels and the content of human or mouse adipocytes within the graft were measured using species-specific endothelial and adipocyte-specific quantitative real time polymerase chain reaction probes, and histochemistry with mouse and human-specific lectins. Our results show that ad-PADS grafted subcutaneously into nude mice induce robust vascularization from the host, continue to increase in volume over time, express the human adipocyte marker *PLIN1* at levels comparable to human AT, and secrete increasing amounts of human adiponectin into the mouse circulation. In contrast, grafts composed of AT fragments obtained by liposuction become less vascularized, develop regions of calcification and decreased content of *PLIN1*, and secrete lower amounts of adiponectin per unit volume. Enrichment of liposuction tissue with ad-PADS improves vascularization, indicating that ad-PADS may be proangiogenic. Mechanistically, ad-PADS express an extracellular matrix gene signature that includes elements previously associated with small vessel development (COL4A1). Thus, through the formation of a proangiogenic environment, ad-PADS can form functional AT with capacity for long-term survival, and can potentially be used to improve outcomes in reconstructive and regenerative medicine.

Keywords: mice, nude, regenerative medicine, adipocytes, adipose tissue, adipogenesis, stem cells, extracellular matrix

Impact Statement

This research describes the use of human mesenchymal progenitor cells for generating functional adipose tissue *in vivo* in a nude mouse model. Further preclinical development of the methods and insights described in this article can lead to therapeutic use of these cells in regenerative and reconstructive medicine.

[1]Program in Molecular Medicine, University of Massachusetts Medical School, Worcester, Massachusetts.
[2]Department of Surgery, University of Massachusetts Medical School and UMASS Memorial Medical Center, Worcester, Massachusetts.
*Equal contributions.
[†]Co-senior authors.

Introduction

ADIPOSE TISSUE (AT) is uniquely capable of great expansion as a function of chronic excess nutrient consumption. Indeed, AT can expand to comprise up to 70% of human body mass.[1] The capacity of AT to grow and promote angiogenesis has fueled the use of fat grafting in numerous medical contexts.[2–6] For example, AT is used for volume restoration after surgery for breast cancer,[7] for soft tissue reconstruction in acquired or congenital malformations,[8,9] and to fill defects such as cranial fractures or fistulas in cranial neurosurgery.[10–12] In the context of regeneration, mesenchymal cells from AT have been used for numerous purposes, including cardiomyocyte,[13] bowel,[14] tendon, and bone regeneration.[15] In the setting of volume restoration, reabsorption and necrosis of grafted fat are a frequent complication,[16,17] resulting in the need for repeated surgical procedures in >25% of cases. While empirical methods to improve fat grafting outcomes have been identified,[18] a further understanding of the cellular and molecular mechanisms of adult human AT development is required to fully leverage its therapeutic potential.

Human adult AT is enriched in mesenchymal stem cells (known as ADipose stem cells, ADSCs), which are capable of differentiation toward the adipogenic, myogenic, chondrogenic, and osteogenic lineages.[19–21] ADSCs were identified and are routinely obtained from the stromovascular fraction (SVF) of AT and may underlie the capacity of AT to expand, thus playing an important role in the outcome of fat grafting. Indeed, in some studies, supplementation of AT with cells from the SVF, which contains ADSCs, displayed significant improvements in volume retention after grafting,[22] and controlled clinical trials support a specific role for ADSCs in graft improvement.[23] The mechanisms by which ADSCs improve grafting are unclear, but they could function by providing new adipocytes or their vascular support.[24,25] A limitation of the use of ADSCs is that relatively few cells can be obtained by conventional enzymatic digestion, and they display loss of differentiation potential with passaging.[26,27] Thus, the therapeutic use of ADSCs is restricted to instances in which relatively large amounts of AT can be collected.

A potential alternative approach to obtaining AT progenitor cells is to leverage the mechanisms by which AT expands physiologically. Previous studies indicate that development of AT is preceded by the formation of a vascular plexus, and lineage-tracing studies have shown that adipocyte progenitors are localized within the adult AT vasculature.[28–36] These findings suggested the possibility that vascular expansion would be accompanied by adipocyte progenitor proliferation. We tested this hypothesis by culturing human AT explants under proangiogenic conditions that elicited capillary sprout formation, and found concomitant robust proliferation of adipocyte progenitor cells.[37,38] Moreover, adipocytes differentiated from these progenitors affected glucose metabolism when implanted into immunocompromised mice.[38]

We now wish to further understand whether these cells (referred to as primed ADipocyte progenitor cells, PADS) are capable of forming structured, long-lived AT that could be used in surgical applications. In this article, we use quantitative morphometric and biochemical methods to investigate the process by which PADS and adipocytes differentiated from PADS (ad-PADS) form structured, functional AT *in vivo*, and compare it to conventional AT grafting. We also compare the molecular features of PADS and ad-PADS to those of ADSCs and ad-ADSCs and report the results of comparative gene expression analyses that identify unexpected pathways and genes associated with the efficient formation of functional AT *in vivo*.

Results

In vivo, human adipocytes contain large lipid droplets, display insulin responsive hypertrophy and leptin secretion, and display long-term survival. To determine the similarities between adipocytes formed from PADS (ad-PADS) and functional human adipocytes, we quantified their growth over a long time in culture in the absence or presence of insulin. Explants were cultured in Matrigel and EGM2-MV for 14 days, and then switched to Dulbecco's modified Eagle's medium (DMEM)+fetal bovine serum (FBS) containing an adipogenic cocktail of methylisobutylxanthine, dexamethasone, and insulin (MDI). After 3 days, cell cultures were continued in DMEM+FBS, and images obtained at the times shown. We find that ad-PADS survive many weeks in culture, during which they transition from a multilocular to a unilocular phenotype (Fig. 1A) and progressively increase in size. After 14 weeks, cells are mostly unilocular, with abundant, functional mitochondria as seen by staining with the mitochondrial dye Mitotracker Red (Fig. 1B). Insulin promotes adipocyte hypertrophy (Fig. 1C), and stimulates leptin secretion (Fig. 1D), indicating that ad-PADS maintain the morphological and functional properties of human adipocytes.

We then conducted experiments to determine whether ad-PADS would form structured AT *in vivo*. Explants were cultured in Matrigel for 14 days, and single cells obtained by digestion with dispase. Cells were plated onto plastic culture dishes and allowed to reach confluence before being exposed to MDI for 3 days. After further culture for an additional 5 days, a time at which lipid droplets were beginning to become visible, cells were collected using collagenase and trypsin, washed and resuspended in Matrigel, and implanted subcutaneously into the flanks of nude mice. To compare the process of tissue generation by ad-PADS to that of mature AT grafting, a dry liposuction was performed on an excised specimen containing skin and subcutaneous tissue immediately following panniculectomy, and liposuction fragments similarly implanted. Microcomputed tomography (CT) scans taken after 8 weeks (Fig. 2A) revealed areas of low attenuation at the sites of injection of AT fragments (Fig. 2A, bottom panel), and smaller, higher attenuated areas at the sites of injection of ad-PADS (Fig. 2A, top panel). To measure graft functionality, we used a human-specific enzyme-linked immunosorbent assay (ELISA) to measure circulating adiponectin, which reflects viability and vascularization of grafted material. Human adiponectin was detectable in most engrafted mice (Fig. 2B), but remarkably, the amount of adiponectin per unit graft volume was 5–10 times higher in ad-PADS compared to liposuction (Fig. 2C). To better understand the differences in graft functionality, we performed immunohistochemistry on the excised grafts. Visual inspection (Fig. 2D) and quantitative image analysis (Fig. 2E, Supplementary Fig. S1; Supplementary data are available online at http://www.liebertpub.com/tea) of the images revealed large decellularized regions in all grafts formed from liposuction tissue, probably corresponding to

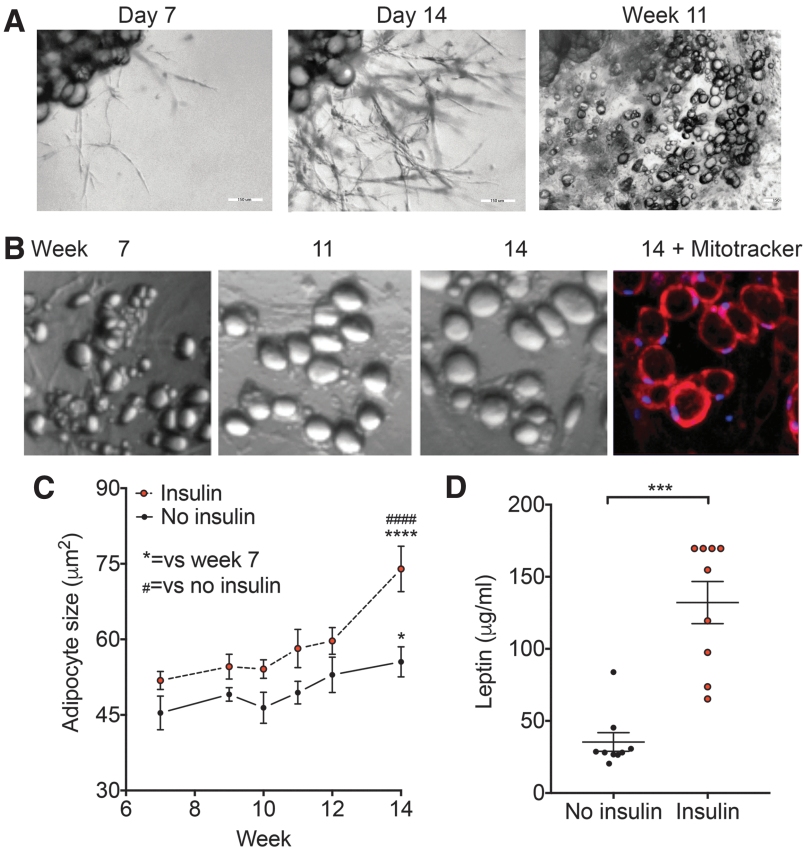

FIG. 1. Development and properties of PADS from human AT explants. **(A)** Representative image of an explant from human subcutaneous AT (*top left corner* of each panel) in culture for the time indicated above each panel. **(B)** Higher magnification of specific section of well, taken at the times indicated. At week 14, Mitotracker *red* was added and cells imaged after 30 min. **(C)** Mean adipocyte size over time, from explants grown in the presence or absence of additional insulin added to the culture medium (100 nM). *Symbols* are the mean and *bars* are SEM of adipocyte sizes, obtained from five independent wells per time point as described in Materials and Methods. Statistical significance was estimated using two-way ANOVA with Dunnett's correction for multiple comparisons. $^{*}p<0.05$, $^{****}p<0.0001$ versus week 7; $^{\#\#\#\#}p<0.0001$ versus no insulin. **(D)** Concentration of leptin in media after 24 h of culture at week 14. Shown are means and SEM of 8–10 wells. Statistical significance was estimated using two-tailed unpaired Mann–Whitney test. $^{***}p<0.001$. ANOVA, analysis of variance; AT, adipose tissue; PADS, primed ADipose progenitor cells; SEM, standard error of the mean.

lipid-filled cysts. These areas were undetectable in grafts formed from ad-PADS (Fig. 2D). These results indicate that ad-PADS are capable of further differentiation and growth *in vivo*, and of efficient functional integration into the host.

To investigate the mechanisms by which PADS integrate into the host, we analyzed the cellular composition of the grafts using quantitative real time polymerase chain reaction (qRT-PCR). We developed species-specific primers to the adipocyte lipid droplet marker perilipin 1 (mouse *Plin1*, human *PLIN1*), and to the mature endothelial cell marker vascular endothelial-cadherin (mouse *Cdh5*, human *CDH5*). Grafts formed from ad-PADS contained equal amount of human *PLIN1* compared to human subcutaneous AT (Fig. 3A), indicating high enrichment of lipid-laden adipocytes. In contrast, grafts formed from liposuction showed marked depletion of *PLIN1*, reflecting loss of functional adipocytes (Fig. 3A). Both types of grafts contained high levels of mouse *Cdh5* (Fig. 3B), reflecting vascularization from the host, but only grafts formed from liposuction tissue contained human *CDH5* (Fig. 3C), indicating that ad-PADS do not differentiate into mature endothelial cells under these conditions.[24] Mouse *Plin1* was very low in both graft types, indicating negligible contamination from the host AT (Fig. 3D). These results indicate that grafts formed from ad-PADS are composed of human adipocytes perfused by mouse vasculature.

The higher survival and functionality of ad-PADS compared to liposuction in the cohort described above could potentially be due by the large difference in volume between the two types of grafts, or by the use of Matrigel during grafting of ad-PADS. The larger volume of liposuction tissue compared to ad-PADS may induce hypoxia (suggested by high levels of *CDH5*), inflammation, and adipocyte death. In addition, Matrigel has autonomous properties that facilitate adipogenesis.[39] To better compare the inherent properties of ad-PADS and liposuction tissue, we performed experiments using smaller volumes of liposuction tissue with the inclusion of Matrigel. In parallel, we examined whether supplementation with ad-PADS would affect the engraftment of liposuction tissue. Three cohorts of mice were randomized to be injected unilaterally subcutaneously with 500 μL of materials as follows: group A—liposuction tissue (250 μL) in Matrigel (250 μL); group B—ad-PADS (100 μL, $\sim 10^7$ cells) in Matrigel (400 μL); and group C—liposuction tissue (225 μL) and ad-PADS (50 μL, $\sim 5\times 10^6$ cells) in Matrigel (225 μL).

Five days following implantation, micro-CT scans revealed areas of low attenuation where liposuction fragments were engrafted (Fig. 4, left top and bottom panels), but the regions where ad-PADS were implanted were not distinguishable, due to their low lipid content at the time of grafting (Fig. 4, left middle panels) and the rapid reabsorption of Matrigel liquid volume after implantation. After 11 and 16 weeks, grafts formed from liposuction fragments had reduced in volume and developed small regions of high attenuation consistent with calcifications (Fig. 4A, right panels, asterisks). In contrast, regions where ad-PADS were implanted were now less attenuated, consistent with further differentiation and lipid accumulation of implanted cells, and no evidence of calcification was seen. At week 16, mice were sacrificed and grafts collected for further analysis. Grafts of liposuction fragments were encapsulated and surrounded by small blood vessels, whereas tissue formed from ad-PADS resembled normal AT (Fig. 4B). Histochemical analysis revealed basophilic structures characteristic of calcification, and large decellularized regions in grafts of liposuction fragments. In contrast, a well-vascularized

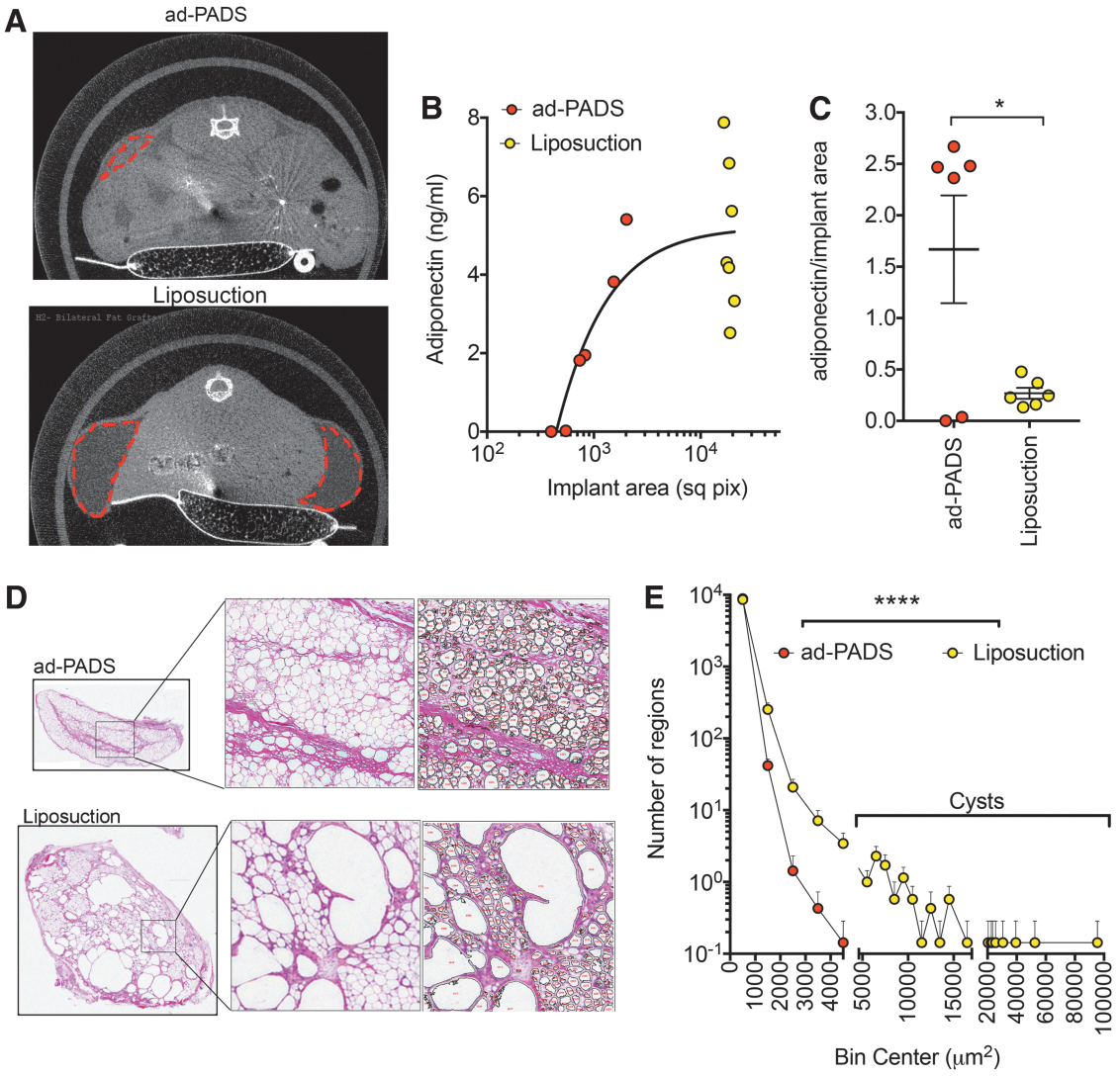

FIG. 2. Comparison of grafts formed from ad-PADS and from liposuction tissue. **(A)** Micro-CT scan of mice implanted with PADS (23 weeks post-implantation, *top panel*) or liposuction tissue (7 weeks post-implantation, *bottom panel*). Areas of low attenuation are enclosed by *red dotted lines*. **(B)** Levels of human adiponectin in plasma from mice implanted as in **(A)**. Each symbol represents the value for each mouse in the cohort. **(C)** Ratio of implant area versus circulating adiponectin. Each symbol represents one mouse, and lines represent the mean and SEM. Statistical significance was estimated using a two-tailed unpaired *t*-test with Welch's correction for unequal standard deviations. $*p<0.05$. **(D)** Histochemical staining of implants formed from PADS (*top panels*) or liposuction tissue (*bottom panels*). Expanded regions illustrate the algorithm output for selection of particles used for quantification. **(E)** Histogram of particle sizes obtained from the mean values of five independent grafts from ad-PADS and seven independent grafts from liposuction tissue. Visual inspection was used to estimate adipocytes as those particles with values lower than between 100 and 5000 μm^2. Statistical significance was estimated using the Friedman test of frequency distributions as implemented in Prism 7.0. $****p<0.0001$. CT, computed tomography.

AT parenchyma distinguishable from the mouse dermal AT was formed from ad-PADS (Fig. 4C).

Analysis of graft volume over time showed a decreasing trend in grafts formed by liposuction fragments, but a significant increase in grafts formed from ad-PADS (Fig. 5A). Functionally, circulating adiponectin significantly increased between weeks 11 and 16 in mice grafted with ad-PADS, but not in mice grafted with liposuction tissue (Fig. 5B). Moreover, ad-PADS were much more efficiently integrated, producing over 10× more adiponectin relative to graft volume (Fig. 5C). These results are consistent with those seen in the first cohort (Fig. 2). Both cohorts were analyzed using a three-component agonist-versus-response fit (Fig 5D). This analysis shows that, at similar graft volumes, ad-PADS produce larger amounts of adiponectin compared to liposuction tissue. Therefore, the enhanced ability of ad-PADS compared to liposuction to induce host vascularization and produce adiponectin cannot be attributed to a smaller graft volume.

To further understand the determinants of graft growth and functionality, we assessed the contributions of donor and host vasculature in each graft type. Both qRT-PCR (Fig. 5E–H) and whole-mount staining with human- and mouse-specific lectins (Fig. 5I) were performed. Grafts formed with liposuction tissue contained high levels of human *CDH5* (Fig. 5G), and vascular staining was detected with human-specific lectin (Fig. 5I), although at a lower

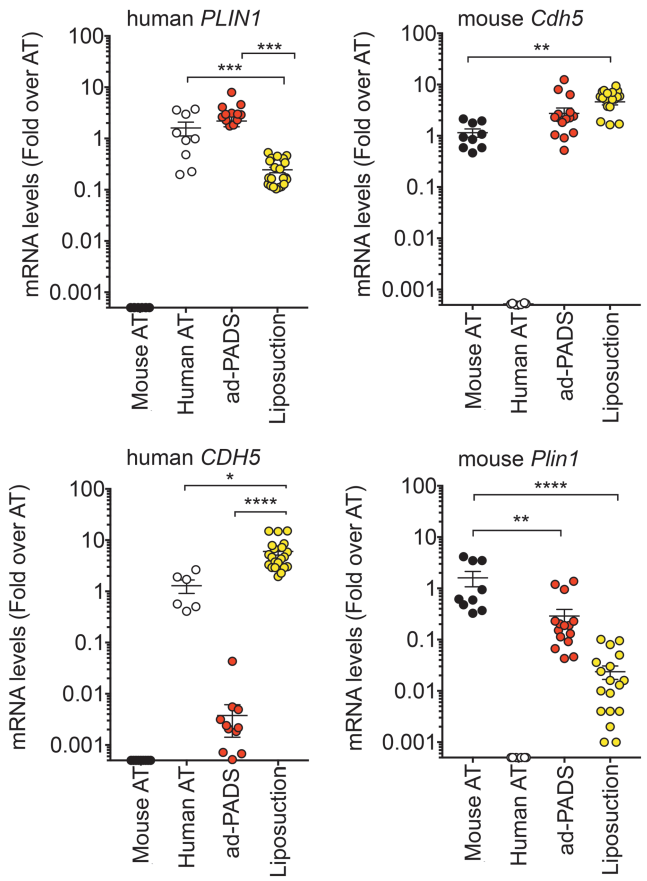

FIG. 3. Human or mouse adipocyte and endothelial cell content in grafts formed from ad-PADS and from liposuction tissue. RNA from excised grafts was analyzed using species-specific RT-PCR probes for the genes indicated above each panel. Symbols represent values for three tissue samples and six to seven grafts per condition assayed in triplicate, and the mean and SEM of all grafts are shown. Statistical significance was estimated using multiple *t*-tests corrected for multiple comparisons using the Holm-Sidak method. *Black circle* indicates mouse adipose tissue; *white circle* indicates human adipose tissue; *red circle* indicates ad-PADS; *yellow circle* indicates liposuction fragments. $*p<0.05$, $**p<0.01$, $***p<0.001$, $****p<0.00001$.

density than that seen in control human AT. Staining with mouse-specific lectin was also seen, but the staining was less well organized than that seen in control mouse tissue or in grafts formed from ad-PADS (Fig. 5I). These grafts also expressed low levels of human *PLIN1* (Fig. 5F), suggesting low adipocyte viability. Grafts formed from ad-PADS contained high levels of mouse *Cdh5* (Fig. 5E), and mouse-specific lectin revealed a well-developed vascular architecture (Fig. 5I), and very high levels of human *PLIN1*. Grafts formed from liposuction tissue supplemented with ad-PADS contained higher levels of mouse *Cdh5* messenger RNA (mRNA) expression (Fig. 5E, compare Liposuction vs. Lipo+ adPADS), and stronger staining with mouse-specific lectin, suggesting a significant proangiogenic effect of these cells.

To better understand the features of PADS, we compared their properties to ADSCs derived from the SVF by standardized procedures as described in Figure 6A. We first measured a panel of classical mesenchymal stem cell markers by qRT-PCR. PADS expressed significantly higher levels of some markers, including PDGFRα, which has been associated with adipocyte progenitors in mouse models, and lower levels of CD24 (Fig. 6B). These differences were sustained after adipogenic differentiation and correlated with increased levels of adipocyte markers (Fig. 6C) and lipid accumulation (Fig. 6D) in ad-PADS. These results indicate that PADS are more enriched in adipocyte progenitors compared to ADSCs.

To compare the properties of ADSCs and PADS *in vivo*, mice were engrafted with equal numbers of these cells. Neither ADSCs nor PADS were able to form a functional AT graft: excised ADSC graft remnants revealed the presence of numerous cell nuclei, but no lipid droplet accumulation (Fig. 6E), while remnants from PADS grafts displayed few lipid droplets. Interestingly, vessel-like structures staining with human-specific lectin (Fig. 6E, arrows), and significantly higher levels of human *CDH5* (Fig. 6F) could be detected in ADSC graft remnants, but not in remnants from PADS, suggesting that ADSCs are capable of forming microvessels *in vivo*. These results above indicate that induction of adipogenic differentiation *in vitro* is absolutely required for PADS to generate functional AT *in vivo*.

To explore the molecular differences between PADS and ad-PADS that could contribute to tissue formation, we conducted HTA-2 Affymetrix whole genome arrays. Of >33,000 mRNAs detected, 269 coding genes were differentially expressed between pre-PADS and PADS (Fig. 6G; Supplementary Table S1). Of these, 40 genes containing the gene ontology cellular component term ''extracellular'' (including ''exosomal'') were upregulated in response to differentiation (Fig. 6H; Table 1). The top biological processes identified through enrichment analysis of this set were ''response to oxygen'' and ''response to wounding'' (Table 2), and included four collagen species (COL4A1, COL5A1, COL3A1, and COL12A1), adhesion proteins (MCAM/CD146, CHL1, and HSPG2), extracellular matrix remodeling proteins (ADAMTS9, OLFM2, and SERPINB2), and secretory hydrolases (PLA2G2A and CH3L2). Also in this list were the expected adipokines and adipocyte-secreted proteins ADIPOQ, FABP4, LPL, FABP5, and RBP4. Interestingly, none of these genes corresponded to known classical proangiogenic growth factors, suggesting that the mechanisms by which PADS are capable of forming functional AT *in vivo* is through the generation of an extracellular matrix niche optimal for adipogenic differentiation and host vascularization.

Discussion

To our knowledge, this article is first to describe a method by which functional, structured human AT can be formed *in vivo* from progenitor cells. The finding that ADSCs can be obtained from human AT has been a critical advancement in regenerative medicine. However, the number of cells that can be obtained is limited; standard methods to obtain ADSCs involve collagenase digestion to obtain the SVF and selection of mesenchymal progenitors through their capacity to attach to plastic surfaces. This can lead to damage from protease action and low yields due to low plating efficiency. A remarkable feature of PADS is that large number of cells can be obtained from small amounts of human AT. Specifically, the number of ADSCs obtained from liposuction tissue varies widely, from

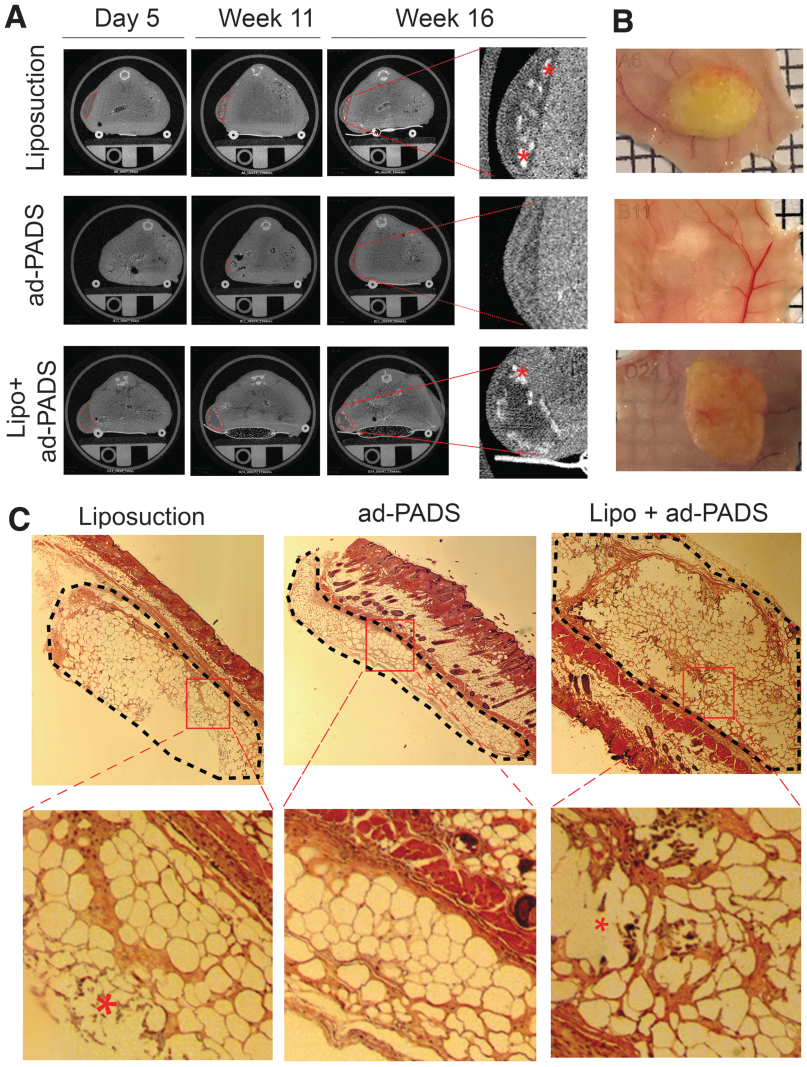

FIG. 4. Development of grafts from ad-PADS and liposuction tissue using comparable volumes. **(A)** Micro-CT scans of mice implanted with liposuction tissue (*top panels*), ad-PADS (*middle panels*), and liposuction tissue supplemented with ad-PADS (*bottom panels*) at the times following grafting indicated on *top*. Areas of low attenuation are outlined with *red dotted traces*, and examples of high attenuation objects within these areas, possibly corresponding to calcifications, are indicated with *asterisks*. **(B)** Macroscopic appearance of grafts at sacrifice. **(C)** Histochemical staining of grafts. Grafted tissue under the skin is outlined with *black*, segmented traces, and basophilic objects within decellularized regions are illustrated with *asterisks* in the expanded images. Examples are representative of seven grafts per condition.

5×10^5 to 2×10^6 cells per gram of AT, with 1 to 10% of these considered to be ADSCs.[15,40] ADSCs expanded in culture cease to replicate after 15 population doublings[41] and display in increasing senescence markers after 4 doublings.[27] Thus, the maximal yield of ADSCs from 1 g of AT can be estimated to be a maximum of 6×10^6 after five passages. In contrast, explants from 0.25 cm^3 ($\sim$200 mg) of AT yielded 2×10^7 cells after 14 days in culture and 8×10^7 adherent cells 72 h after plating in plastic. In our hands, PADS are passaged in a 1:2 split after this step to yield 1.7×10^8 cells, which are frozen and can be expanded through five population doublings with no decrease in adipose differentiation capacity. Therefore $\sim5\times10^9$ PADS can be obtained from 1 g of human AT, representing a 1000$\times$higher yield than ADSCs. It is possible that three-dimensional (3D) organ culture triggers a physiological induction of progenitor cell proliferation, which in combination with minimal damage from mechanical or chemical stress leads to very high yields of mesenchymal progenitor cells.

The differences between ADSCs and PADS extend beyond the yield of cells obtained through different techniques, as cell surface marker content differs significantly (Fig. 6B, C) as do functional outcomes. It is interesting that ADSCs seem more capable of producing vascular structures *in vivo* (Fig. 6E, F), consistent with numerous reports of their proangiogenic effects.[42–47] In contrast, PADS are more able to differentiate into adipocytes, and can induce host angiogenesis. These functional differences are likely due to the different complement of cells making up the ADSC and PADS populations.

An important finding in this study is that the ability to form structured AT *in vivo* is highly dependent on prior induction of adipogenic differentiation *in vitro*. Comparison of PADS and ad-PADS can thus inform on the biochemical pathways important for tissue generation. As expected, the most significant biological pathways enriched in ad-PADS compared to PADS are related to canonical AT function, with the top 20 corresponding to lipid metabolic processes, including storage and catabolism. However, the first non-lipid related pathway significantly enriched is that of wound healing (Supplementary Table S2). When the differentially expressed genes are restricted to those associated with the extracellular compartment, the second most enriched pathway corresponds to wound healing (Table 2). Strikingly, none of the genes previously associated with angiogenesis in the context of ADSCs, which include VEGF FGF-2, HGF, and TGF-β,[48] was found. Rather, extracellular matrix components, including five different collagen types, were the predominant associated genes. One of these, COL4A1, is essential for small vessel development and pathogenic mutations cause vascular

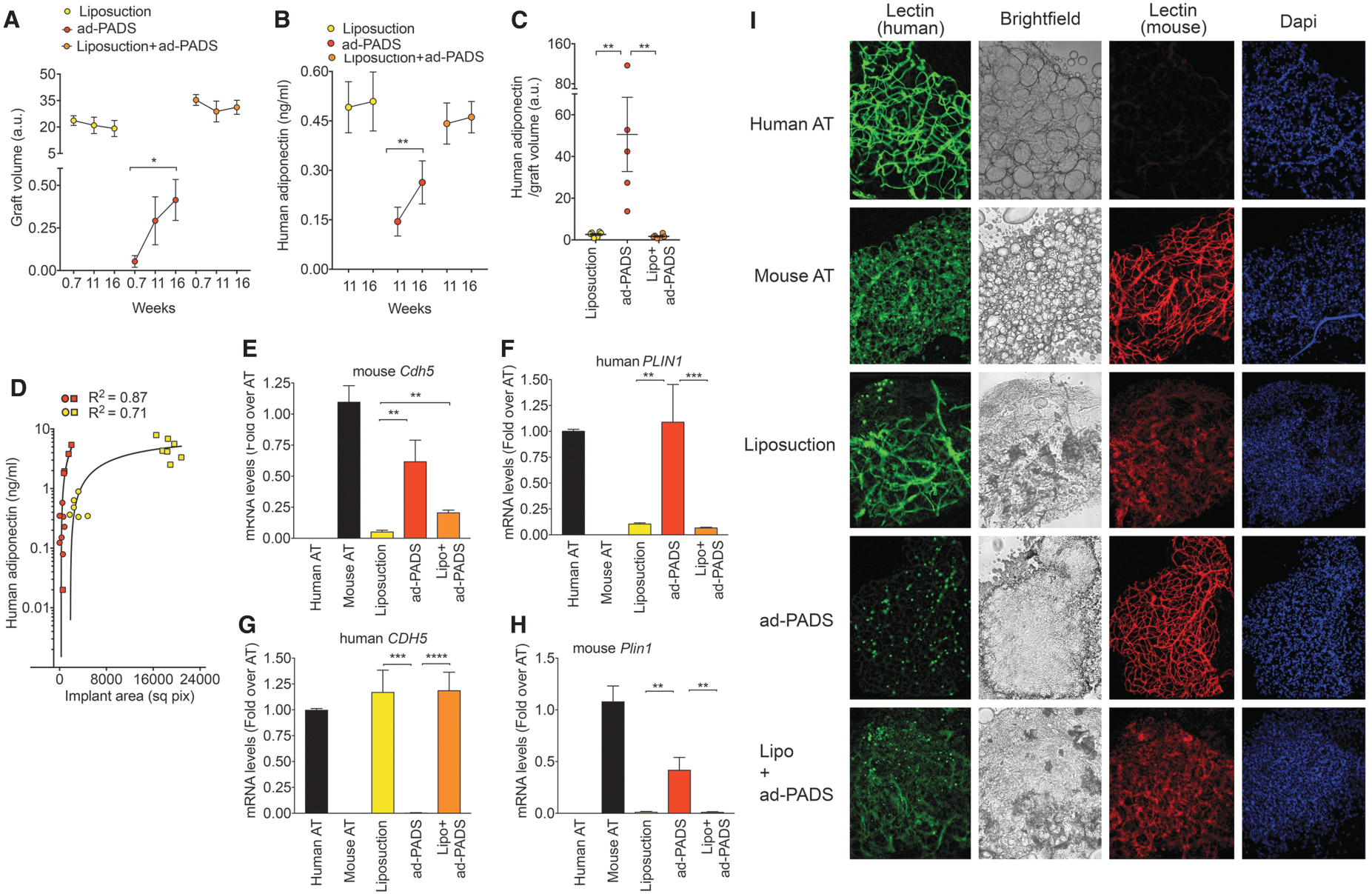

FIG. 5. Quantification of graft volume, functionality, and endothelial or adipose cell content. **(A)** Mean and SEM of graft volumes calculated from micro-CT scans, and **(B)** mean and SEM of human adiponectin in plasma, obtained at the times shown on the *x*-axes, from seven mice per condition implanted with liposuction tissue, ad-PADS, or liposuction tissue supplemented by ad-PADS. Statistical significance was estimated using paired *t*-tests. $*p<0.05$, $**p<0.01$. **(C)** Mean and SEM of the ratios of human adiponectin to graft volumes at 16 weeks postgrafting in mice harboring grafts from liposuction tissue, ad-PADS, or liposuction tissue supplemented by ad-PADS. Statistical significance was estimated using one-way ANOVA with Tukey's correction for multiple comparisons, $**p<0.01$. **(D)** Relationship between graft volume and plasma adiponectin in mice from cohorts 1 (*squares*) and 2 (*circles*). Each symbol corresponds to values from one mouse. **(E–H)** RNA from excised grafts was analyzed using species-specific qRT-PCR probes for the genes indicated above each panel. Bars represent the mean and lines the SEM of all grafts. Statistical significance was estimated using the Krustal–Wallis test with Dunnett's correction for multiple comparisons. $**p<0.01$, $***p<0.001$, $****p<0.00001$. **(I)** Whole-mount staining of fragments from control human and mouse AT, and from grafts formed from liposuction tissue, ad-PADS, or liposuction tissue supplemented by ad-PADS, costained with mouse- and human-specific lectins and DAPI. DAPI, 4′,6-diamidino-2-phenylindole (nuclear staining); mRNA, messenger RNA; qRT-PCR, quantitative real time polymerase chain reaction.

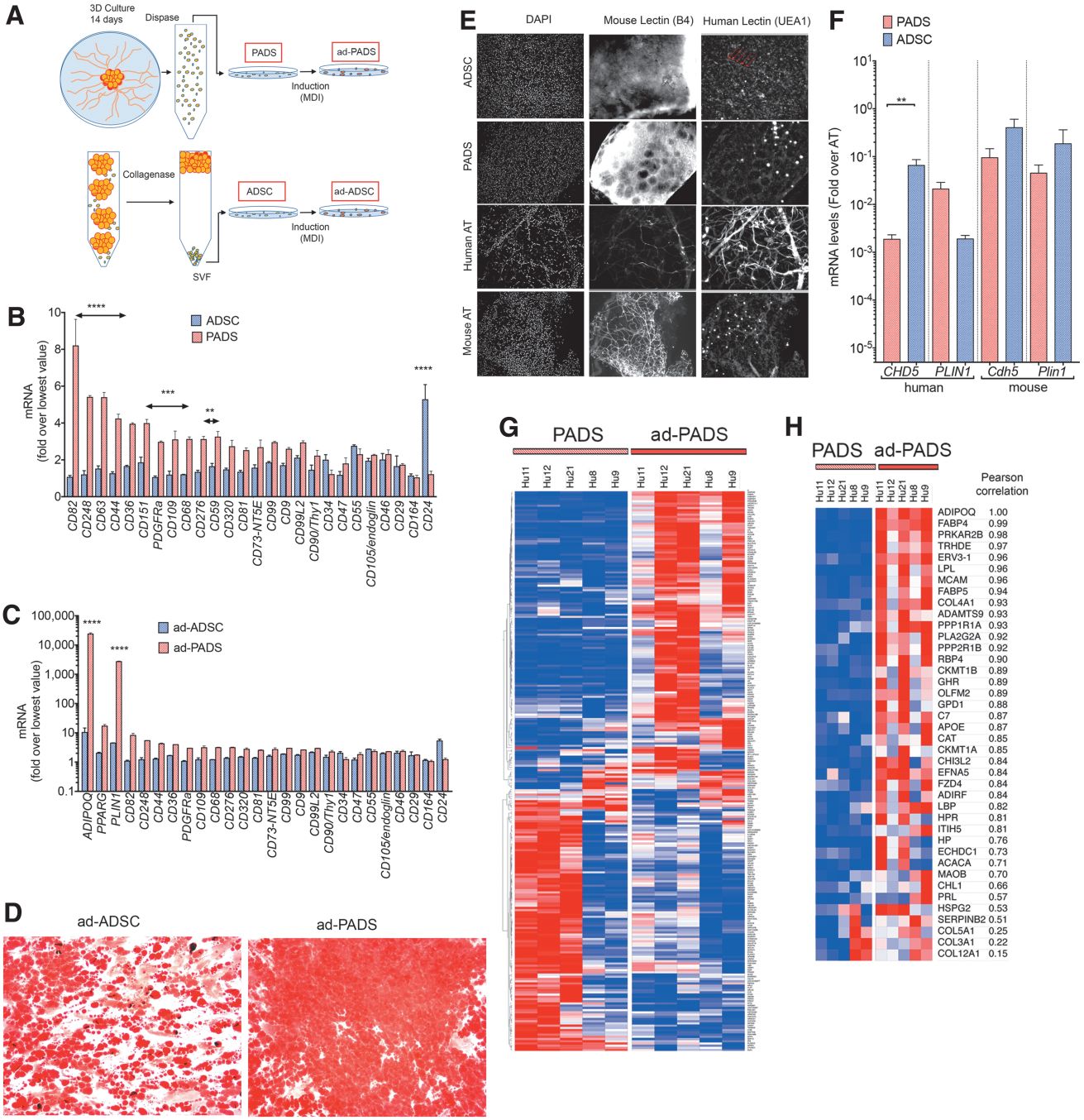

FIG. 6. Molecular features associated with tissue formation. **(A)** Schematic representing the methods to obtain PADS, ad-PADS, ADSCs, and ad-ADSCs. **(B, C)** RNA from two independent preparations of PADS, ad-PADS, ADSCs, and ad-ADSCs was probed for the mesenchymal stem cell **(B, C)** and adipocyte **(C)** markers depicted on the *x*-axis. Values are expressed as the fold over the lowest value for each probe set. Statistical significance was estimated using multiple *t*-tests corrected for multiple comparisons using the Holm-Sidak method. *Double headed arrows* are placed over sets of probes that differed significantly, at the levels indicated $^{**}p<0.01$, $^{***}p<0.001$, $^{****}p<0.00001$. **(D)** Oil Red O staining of ad-ADSCs and ad-PADS after 10 days of differentiation. **(E)** Whole-mount costaining of grafts formed from ADSCs and PADS using DAPI, and mouse- and human-specific lectins. Control human and mouse AT are included for comparison. Linear structures stained with human-specific lectin in grafts formed from ADSCs are indicated with *red arrows*. **(F)** RNA from excised grafts was analyzed using species-specific qRT-PCR probes for the genes indicated on the *x*-axis. *Bars* represent the mean, and *lines* the SEM of seven grafts per condition assayed in duplicate. Statistical significance was estimated using the Krustal–Wallis test with Dunnett's correction for multiple comparisons. $^{**}p<0.01$. **(G)** Heat map of differentially expressed genes between PADS and ad-PADS, obtained from AT from five different individuals. **(H)** Heat map of differentially expressed genes containing the GO term ''extracellular.'' ADSCs, ADipose stem cells.

Table 1. Genes Containing the Gene Ontology:Cell Component Term "Extracellular" That are Upregulated in ad-Primed ADipose Progenitor Cells (PADS) Compared to PADS

	Biweight Average signal (Log2)					
Gene symbol	*pre-PADS*	*PADS*	*Fold change (linear)*	*ANOVA* p-*value*	*FDR* p-*value*	*Description*
COL12A1	15.62	16.63	2.02	0.034278	0.738561	Collagen, type XII, alpha 1
COL3A1	14.76	15.83	2.1	0.014497	0.706983	Collagen, type III, alpha 1
ADIPOQ	6.02	14.15	278.53	0.001938	0.63372	Adiponectin
PPP2R1B	9.85	12.13	4.83	0.012173	0.706983	Protein phosphatase 2, regulatory subunit A, beta
ERV3-1	9.04	11.89	7.22	0.001606	0.63372	Endogenous retrovirus group 3, member 1; zinc finger protein 117
HSPG2	10.6	11.75	2.22	0.011174	0.702326	Heparan sulfate proteoglycan 2
ACACA	8.75	11.6	7.2	0.035299	0.738561	Acetyl-CoA carboxylase alpha
CAT	9.87	11.22	2.56	0.01749	0.717727	Catalase
LPL	4.61	11.06	87.66	0.008961	0.697682	Lipoprotein lipase
ECHDC1	9.19	11.01	3.52	0.030393	0.730714	Ethylmalonyl-CoA decarboxylase 1
HP	5	10.98	63.29	0.007908	0.694757	Haptoglobin
C7	7.59	10.97	10.39	0.023862	0.725644	Complement component 7
RBP4	7.18	10.59	10.6	0.019018	0.720701	Retinol binding protein 4, plasma
FZD4	8.85	10.56	3.27	0.035148	0.738561	Frizzled class receptor 4
OLFM2	8.37	10.53	4.47	0.003836	0.640504	Olfactomedin 2
COL4A1	8.43	10.19	3.37	0.049268	0.765581	Collagen, type IV, alpha 1
PLA2G2A	7.93	10.06	4.38	0.011995	0.70568	Phospholipase A2, group IIA (platelets, synovial fluid)
CHI3L2	6.32	9.95	12.39	0.000282	0.453651	Chitinase 3-like 2
MCAM	5.94	9.87	15.28	0.012533	0.706983	Melanoma cell adhesion molecule
GHR	6.74	9.76	8.12	0.014529	0.706983	Growth hormone receptor
LBP	5.63	9.7	16.82	0.011861	0.70411	Lipopolysaccharide binding protein
GPD1	5.6	9.42	14.16	0.009315	0.69817	Glycerol-3-phosphate dehydrogenase 1
PRKAR2B	6.2	9.41	9.23	0.007145	0.68923	Protein kinase, cAMP-dependent, regulatory, type II, beta
CHL1	7.79	9.02	2.35	0.042315	0.752979	Cell adhesion molecule L1 like
COL5A1	7.58	8.62	2.06	0.045381	0.756446	Collagen, type V, alpha 1
FABP5	5.73	8.46	6.6	0.011525	0.702953	Fatty acid binding protein 5 (psoriasis associated)
ADIRF	6.54	8.29	3.36	0.020917	0.724127	Adipogenesis regulatory factor
EFNA5	6.89	8.14	2.37	0.016816	0.717167	Ephrin-A5
PRL	5.67	7.91	4.72	0.001102	0.625574	Prolactin
APOE	6.45	7.71	2.4	0.038401	0.742836	Apolipoprotein E
ITIH5	6.35	7.67	2.51	0.005753	0.666918	Inter-alpha-trypsin inhibitor heavy chain family, member 5
HPR	5.36	7.32	3.9	0.012947	0.706983	Haptoglobin-related protein; haptoglobin
SERPINB2	5.66	7.13	2.78	0.043889	0.752979	Serpin peptidase inhibitor, clade B (ovalbumin), member 2
MAOB	5.48	6.65	2.24	0.0157	0.711636	Monoamine oxidase B
ADAMTS9	4.89	6.57	3.23	0.003176	0.63372	ADAM metallopeptidase with thrombospondin type 1 motif 9
TRHDE	4.77	6.51	3.36	0.014351	0.706983	Thyrotropin-releasing hormone-degrading enzyme
CKMT1B	5.17	6.22	2.07	0.042988	0.752979	Creatine kinase, mitochondrial 1B; creatine kinase, mitochondrial 1A
PPP1R1A	5.19	6.21	2.03	0.015221	0.711636	Protein phosphatase 1, regulatory (inhibitor) subunit 1A
CKMT1A	4.42	5.53	2.15	0.049139	0.765232	Creatine kinase, mitochondrial 1A; creatine kinase, mitochondrial 1B

The signals are means from five independent arrays, and values are sorted based on intensity of signal in ad-PADS.
ANOVA, analysis of variance; FDR, false discovery rate; PADS, primed ADipose progenitor cells.

abnormalities,[49–52] suggesting it may have an important role in vascularization of PADS for engraftment. Also, mutations in COL3A1 give rise to vascular Ehlers–Danlos syndrome,[53] indicating a role for this collagen type in vascular integrity. Other identified genes include MCAM/CD146, which has been implicated in lymphangiogenesis,[54] brain endothelial cell functions,[55] and angiogenesis.[56,57] The interactions among these genes may also be critically important for tissue development, as has been reported for the morphogenesis of vascular structures through interactions between ADAMTS9 with

Table 2. Biological Processes Showing Enrichment of Genes Containing the Gene Ontology:Cell Component Term ''Extracellular'' That are Upregulated in ad-Primed ADipose Progenitor Cells (PADS) Compared to PADS

GO biological process ID	*Name*	p-*value*	q-*value Bonferroni*	*Hit count in query list*	*Hit count in genome*	*Hit in query list*
GO:1901700	Response to oxygen-containing compound	6.49E-09	1.23E-05	17	1614	COL3A1, FZD4, COL4A1, GHR, GPD1, PRKAR2B, CAT, LBP, ADIPOQ, EFNA5, APOE, ACACA, MAOB, HP, PRL, LPL, RBP4
GO:0009611	Response to wounding	4.24E-08	8.06E-05	13	967	CHL1, COL3A1, MCAM, PLA2G2A, PRKAR2B, COL5A1, LBP, ADIPOQ, C7, APOE, LPL, FABP5, SERPINB2
GO:0044236	Multicellular organism Metabolic process	5.09E-07	9.68E-04	6144		COL3A1, COL4A1, GHR, COL5A1, COL12A1, ACACA
GO:0044255	Cellular lipid metabolic process	1.06E-06	2.01E-03	12	1064	GHR, GPD1, PLA2G2A, PRKAR2B, HSPG2, CAT, ADIPOQ, APOE, ACACA, LPL, FABP5, RBP4
GO:0006600	Creatine metabolic	1.39E-06	2.63E-03	3	11	GHR, CKMT1B, CKMT1A
GO:0006641	Triglyceride metabolic process	4.01E-06	7.62E-03	5	115	GPD1, CAT, APOE, LPL, FABP5
GO:1901701	Cellular response to oxygen-containing compound	4.27E-06	8.12E-03	11	1001	COL3A1, FZD4, COL4A1, GHR, GPD1, PRKAR2B, LBP, ADIPOQ, EFNA5, ACACA, PRL
GO:0044259	Multicellular organismal macromolecule	6.52E-06	1.24E-02	5	127	COL3A1, COL4A1, COL5A1, COL12A1, ACACA
GO:0006639	Acylglycerol metabolic process	6.77E-06	1.29E-02	5	128	GPD1, CAT, APOE, LPL, FABP5

GO, gene ontology.

HSPG2.[58,59] How these genes exert these specific actions is not known, but the use of ad-PADS grafting as a model may be useful for elucidating their molecular functions.

The therapeutic use of ad-PADS is an exciting prospect in reconstructive surgery, particularly in instances such as wound healing or restoration of soft tissue volume after cancer surgery. Ad-PADS could be used alone for small reconstructive requirements or in combination with liposuction tissue to enhance large volume grafting. In our study, supplementation of liposuction tissue with PADS significantly enhanced vascularization, and further experiments will determine whether an optimal ratio of ad-PADS to tissue can achieve functionally improved grafting. The therapeutic use of PADS could extend beyond reconstructive surgery. For example, in congenital generalized lipodystrophies, there is a virtual absence of adiponectin and leptin due to genetic defects preventing adipose differentiation. PADS from these subjects could be corrected *in vitro*, and autologous implantation of *in vitro*-generated ad-PADS could potentially ameliorate endocrine pathology in these cases.

The limitations of this work are that, like ADSCs, PADS are heterogeneous, and we cannot fully describe their complexity or identify the specific complement of cells required for AT formation *in vivo*. This next step will require the development of methods to identify and enrich the different progenitor subpopulations, and to examine their ability to engraft singly or in combinations. Nevertheless, the capacity of PADS to form functional AT has been reproduced in our laboratory with a minimum of 5 different cell preparations from different donors, using both NSG[38] and nude mouse strains (current results), indicating robust conserved mechanisms at play. An additional limitation is the use of Matrigel for 3D expansion of PADS. Identification of good manufacturing practice-compliant hydrogels that can replace Matrigel is a necessary step in using ad-PADS to improve therapeutic outcomes.

In summary, this article demonstrates that ad-PADS can form structured AT *in vivo* by inducing strong vascularization from the host and continued human adipocyte growth and differentiation. Enrichment of liposuction with ad-PADS improves vascularization, indicating that ad-PADS may be proangiogenic, possibly through expression of extracellular matrix elements previously associated with small vessel development. The capacity to generate very large numbers of PADS from small amounts of AT increases their potential to improve outcomes in reconstructive and regenerative medicine.

Materials and Methods

Specific reagents

Matrigel (BD Biosciences); EGM-2 MV (Lonza); Adiponectin human-specific ELISA (Invitrogen KHP0041);

Rhodamine Ulex europaeus Agglutinin 1 (Vector labs RL-1062); and Isolectin GS IB4 Alexa Fluor 488 Conjugate (Life Technologies I21411).

Adipose tissue

Subcutaneous AT for grafting and for derivation of PADS was obtained from panniculectomies with no a priori selection of individual donors. All specimens were collected in accordance with procedures approved by the University of Massachusetts Institutional Review Board (IRB).

Liposuction tissue

Tissue was obtained from panniculectomies performed at our institution, under an approved IRB. Immediately after excision of the panniculus from the patient, AT was extracted manually in multiple passes with a 3 mm cannula, and centrifuged at 3000 RPM for 3 min. Aqueous and lipid components were discarded and fat used for grafting directly, or after mixing with an equal volume of Matrigel by gentle inversion, as indicated in each experiment. In some experiments, the 50/50 mixture of liposuction tissue and Matrigel was supplemented with PADS as described in the Results section.

Cells

Detailed methods for harvesting AT, culture of AT explants in Matrigel, and harvesting of single cells from explant growth are published.[60] In brief, explants from human subcutaneous AT were cultured in EBM-2 media supplemented with endothelial growth factors (EGM-2 MV) (Lonza) for 14 days. Single-cell suspensions from capillary growth were obtained using dispase (yield $\sim 2 \times 10^7$ cells from one 10 cm plate) and plated into two 15 cm tissue culture dish. After 72 h, cells were split 1:2, grown for an additional 72 h, recovered by trypsinization (yield $\sim 8 \times 10^7$), and frozen into 10 vials. To generate PADS for grafting, single vials were thawed out and plated into 1×150 mm dish per graft and grown to confluence in EGM-2 MV. Differentiation was induced by replacement of EGM-2 MV by DMEM +10% FBS, 0.5 mM 3-isobutyl-1-methylxanthine, 1 μM dexamethasone, and 1 μg/mL insulin (MDI). Seventy-two hours later, the differentiation medium was replaced by DMEM-FBS, which was replaced every 48 h for 10 days.

Mice

All animal use was in accordance with the guidelines of the Animal Care and Use Committee of the University of Massachusetts Medical School. Male nude mice were obtained from the Charles River Laboratories. Liposuction tissue, PADS, or a combination as indicated were grafted subcutaneously into the flank 5 cm cephalad to the tail and 3 cm lateral to the spine. Under sterile conditions, an 18G IV cannula was used to penetrate the skin at the base of the tail of each mouse. The needle was withdrawn and the shield of the catheter was advanced to the selected area, creating a tunnel by blunt dissection. A semirigid circular-shaped plastic splint with a central hole of 1.5 cm diameter was positioned on the skin encircling the selected area to be grafted, to ensure proper location and prevent displacement of the graft at the time of injection. The splint was left in place for 3 days and then removed. Serial volumetric analysis by micro-CT scanning was performed as described.[61] Immediately after euthanasia, grafts were dissected, and half of the graft was fixed in 4% paraformaldehyde for microscopy and half used for RNA extraction using TRIzol. For RT-PCR, total RNA was reverse transcribed using the iScript cDNA Synthesis Kit (Bio-Rad). cDNA was used as template for qRT-PCR using the iQ SYBR Green Supermix Kit (Bio-Rad) and the CFX96 Real-Time System (Bio-Rad). Human ribosomal protein L4 (RPL4) was used for normalization.

Gene expression

For RT-PCR, total RNA was reverse transcribed using the iScript cDNA Synthesis Kit (Bio-Rad). cDNA was used as template for qRT-PCR using the iQ SYBR Green Supermix Kit (Bio-Rad) and the CFX96 Real-Time System (Bio-Rad). RPL4 was used for normalization. Human- and mouse-specific probe sets are shown in Supplementary Table S3. For Affymetrix arrays, total RNA was isolated using TRIzol, from pre-PADS and PADS obtained from five independent subjects. Affymetrix protocols were followed for the preparation of cRNA, which was hybridized to HTA-2.0 arrays. Raw expression data collected from an Affymetrix HP GeneArrayScanner were normalized across all data sets using the robust multi-array algorithm as implemented by the Affymetrix Expression Console. Differential expression analysis was performed using the Affymetrix Transcriptome Analysis Console v.3.0. Pathway analysis of transcriptomic data was performed using ToppGene.[62]

Histochemistry and quantification

Samples were fixed in 4% formaldehyde and embedded in paraffin. Tissue sections (8-μm), were mounted on Superfrost Plus microscope slides (Fisher Scientific) and stained with hematoxylin and eosin; $10\times$ images were taken using brightfield microscopy (Zeiss Axiovert 35) and AxioCam Icc 1 digital camera (Zeiss). Adipocyte (area) size was determined using an automated procedure based on the open software platform FIJI.[63] In brief, images were imported, local contrast enhanced (CLAHE, blocksize = 263, histogram = 256, maximum = 40), converted to 8-bit grayscale image, binarized (threshold 136, 255, dark background), eroded (iterations = 1, count = 6, black, pad do = Erode), and object number and size were measured (Analyze Particles, size = 100-Infinity circularity = 0.10–1.00). Frequency distributions were obtained for each section using a bin size of 1000, and the mean and standard error of the mean for each bin were calculated to generate the composite histogram for each graft type. For whole-mount staining, tissue fragments were fixed in 4% formaldehyde, washed, and stained with a mixture of 50 μg/mL each Rhodamine Ulex europaeus Agglutinin 1 (Vector labs RL-1062) and Isolectin GS IB4 Alexa Fluor 488 Conjugate (Life Technologies I21411) for 1 h at room temperature. After washing in phosphate-buffered saline, fragments were mounted between 1.5 mm coverslips sealed with ProLong Gold Antifade Reagent (Life Technologies).

Statistical analysis

GraphPad Prism 7.0 was used for all analyses. Parametric or nonparametric test were chosen based on results from the D'Agostino-Pearson omnibus normality test, and are described in each figure.

Acknowledgments

This work was supported by grant DK089101-04 to S.C., and a Pilot Project grant from UL1 TR000161-05 to S.C. and J.L.

Disclosure Statement

Silvia Corvera is a consultant for Glory Harvest Group which has licensed intellectual property from UMASS Medical School.

References

1. Parlee, S.D., Lentz, S.I., Mori, H., and MacDougald, O.A. Quantifying size and number of adipocytes in adipose tissue. Methods Enzymol **537,** 93, 2014.
2. Simonacci, F., Bertozzi, N., and Raposio, E. Off-label use of adipose-derived stem cells. Ann Med Surg (Lond) **24,** 44, 2017.
3. Minteer, D.M., Marra, K.G., and Rubin, J.P. Adipose stem cells: biology, safety, regulation, and regenerative potential. Clin Plast Surg **42,** 169, 2015.
4. Nery, A.A., Nascimento, I.C., Glaser, T., Bassaneze, V., Krieger, J.E., and Ulrich, H. Human mesenchymal stem cells: from immunophenotyping by flow cytometry to clinical applications. Cytometry A **83,** 48, 2013.
5. Yoshimura, K., Sato, K., Aoi, N., *et al.* Cell-assisted lipotransfer for facial lipoatrophy: efficacy of clinical use of adipose-derived stem cells. Dermatol Surg **34,** 1178, 2008.
6. Matsumoto, D., Sato, K., Gonda, K., *et al.* Cell-assisted lipotransfer: supportive use of human adipose-derived cells for soft tissue augmentation with lipoinjection. Tissue Eng **12,** 3375, 2006.
7. van Turnhout, A.A., Fuchs, S., Lisabeth-Broné, K., Vriens-Nieuwenhuis, E.J.C., and van der Sluis, W.B. Surgical outcome and cosmetic results of autologous fat grafting after breast conserving surgery and radiotherapy for breast cancer: a retrospective cohort study of 222 fat grafting sessions in 109 patients. Aesthet Plast Surg **41,** 1334, 2017.
8. Stewart, D.A., Taylor, K.O., Johnstone, B.R., and Coombs, C.J. Structural fat grafting to improve aesthetic outcomes in congenital hand surgery. Plast Reconstr Surg **130,** 386e, 2012.
9. Ogino, T., Ishigaki, D., Satake, H., and Iba, K. Free fat graft for congenital hand differences. Clin Orthop Surg **4,** 45, 2012.
10. Zaidi, H.A., Pendleton, C., Cohen-Gadol, A.A., and Quinones-Hinojosa, A. Harvey Cushing's repair of a dural defect after a traumatic brain injury: novel use of a fat graft. World Neurosurg **75,** 696, 2011.
11. Feroze, A.H., Walmsley, G.G., Choudhri, O., Lorenz, H.P., Grant, G.A., and Edwards, M.S. Evolution of cranioplasty techniques in neurosurgery: historical review, pediatric considerations, and current trends. J Neurosurg **123,** 1098, 2015.
12. Di Vitantonio, H., De Paulis, D., Del Maestro, M., *et al.* Dural repair using autologous fat: our experience and review of the literature. Surg Neurol Int **7(Suppl. 16),** S463, 2016.
13. Roura, S., Gálvez-Montón, C., Mirabel, C., Vives, J., and Bayes-Genis, A. Mesenchymal stem cells for cardiac repair: are the actors ready for the clinical scenario? Stem Cell Res Ther **8,** 238, 2017.
14. Zhang, X.M., Zhang, Y.J., Wang, W., Wei, Y.Q., and Deng, H.X. Mesenchymal stem cells to treat Crohn's disease with fistula. Hum Gene Ther **28,** 534, 2017.
15. Pak, J., Lee, J.H., Park, K.S., Park, M., Kang, L.W., and Lee, S.H. Current use of autologous adipose tissue-derived stromal vascular fraction cells for orthopedic applications. J Biomed Sci **24,** 9, 2017.
16. Laloze, J., Varin, A., Gilhodes, J., *et al.* Cell-assisted lipotransfer: friend or foe in fat grafting? Systematic review and meta-analysis. J Tissue Eng Regen Med 12**,** e1237, 2018.
17. Simonacci, F., Grieco, M.P., Bertozzi, N., and Raposio, E. Autologous fat transplantation for secondary breast reconstruction: our experience. G Chir **38,** 117, 2017.
18. Strong, A.L., Cederna, P.S., Rubin, J.P., Coleman, S.R., and Levi, B. The current state of fat grafting: a review of harvesting, processing, and injection techniques. Plast Reconstr Surg **136,** 897, 2015.
19. De Ugarte, D.A., Morizono, K., Elbarbary, A., *et al.* Comparison of multi-lineage cells from human adipose tissue and bone marrow. Cells Tissues Organs **174,** 101, 2003.
20. Zuk, P.A., Zhu, M., Ashjian, P., *et al.* Human adipose tissue is a source of multipotent stem cells. Mol Biol Cell **13,** 4279, 2002.
21. Gronthos, S., Franklin, D.M., Leddy, H.A., Robey, P.G., Storms, R.W., and Gimble, J.M. Surface protein characterization of human adipose tissue-derived stromal cells. J Cell Physiol **189,** 54, 2001.
22. Toyserkani, N.M., Quaade, M.L., and Sørensen, J.A. Cell-assisted lipotransfer: a systematic review of its efficacy. Aesthet Plast Surg **40,** 309, 2016.
23. Kølle, S.F., Fischer-Nielsen, A., Mathiasen, A.B., *et al.* Enrichment of autologous fat grafts with ex-vivo expanded adipose tissue-derived stem cells for graft survival: a randomised placebo-controlled trial. Lancet **382,** 1113, 2013.
24. Planat-Benard, V., Silvestre, J.S., Cousin, B., *et al.* Plasticity of human adipose lineage cells toward endothelial cells: physiological and therapeutic perspectives. Circulation **109,** 656, 2004.
25. Miranville, A., Heeschen, C., Sengenès, C., Curat, C.A., Busse, R., and Bouloumié, A. Improvement of postnatal neovascularization by human adipose tissue-derived stem cells. Circulation **110,** 349, 2004.
26. Dao, L.T., Park, E.Y., Hwang, O.K., Cha, J.Y., and Jun, H.S. Differentiation potential and profile of nuclear receptor expression during expanded culture of human adipose tissue-derived stem cells reveals PPARgamma as an important regulator of Oct4 expression. Stem Cells Dev **23,** 24, 2014.
27. Legzdina, D., Romanauska, A., Nikulshin, S., Kozlovska, T., and Berzins, U. Characterization of senescence of culture-expanded human adipose-derived mesenchymal stem cells. Int J Stem Cells **9,** 124, 2016.
28. Jiang, Y., Berry, D.C., Jo, A., *et al.* A PPARgamma transcriptional cascade directs adipose progenitor cell-niche interaction and niche expansion. Nat Commun **8,** 15926, 2017.
29. Corvera, S., and Gealekman, O. Adipose tissue angiogenesis: impact on obesity and type-2 diabetes. Biochim Biophys Acta **1842,** 463, 2014.
30. Tran, K.V., Gealekman, O., Frontini, A., *et al.* The vascular endothelium of the adipose tissue gives rise to both white and brown fat cells. Cell Metab **15,** 222, 2012.

31. Lin, G., Liu, G., Banie, L., *et al.* Tissue distribution of mesenchymal stem cell marker Stro-1. Stem Cells Dev **20,** 1747, 2011.
32. Cai, X., Lin, Y., Hauschka, P.V., and Grottkau, B.E. Adipose stem cells originate from perivascular cells. Biol Cell **103,** 435, 2011.
33. Crisan, M., Yap, S., Casteilla, L., *et al.* A perivascular origin for mesenchymal stem cells in multiple human organs. Cell Stem Cell **3,** 301, 2008.
34. Cinti, S., and Morroni, M. Brown adipocyte precursor cells: a morphological study. Ital J Anat Embryol **100(Suppl. 1),** 75, 1995.
35. Jiang, Y., Berry, D.C., Tang, W., and Graff, J.M. Independent stem cell lineages regulate adipose organogenesis and adipose homeostasis. Cell Rep **9,** 1007, 2014.
36. Tang, W., Zeve, D., Suh, J.M., *et al.* White fat progenitor cells reside in the adipose vasculature. Science **322,** 583, 2008.
37. Gealekman, O., Gurav, K., Chouinard, M., *et al.* Control of adipose tissue expandability in response to high fat diet by the insulin-like growth factor-binding protein-4. J Biol Chem **289,** 18327, 2014.
38. Min, S.Y., Kady, J., Nam, M., *et al.* Human ''brite/beige'' adipocytes develop from capillary networks, and their implantation improves metabolic homeostasis in mice. Nat Med **22,** 312, 2016.
39. Kitagawa, Y., and Kawaguchi, N. De novo adipogenesis for reconstructive surgery. Cytotechnology **31,** 29, 1999.
40. Baer, P.C., and Geiger, H. Adipose-derived mesenchymal stromal/stem cells: tissue localization, characterization, and heterogeneity. Stem Cells Int **2012,** 812693, 2012.
41. Burrow, K.L., Hoyland, J.A., and Richardson, S.M. Human adipose-derived stem cells exhibit enhanced proliferative capacity and retain multipotency longer than donor-matched bone marrow mesenchymal stem cells during expansion *in vitro*. Stem Cells Int **2017,** 2541275, 2017.
42. Chen, Y.L., Sun, C.K., Tsai, T.H., *et al.* Adipose-derived mesenchymal stem cells embedded in platelet-rich fibrin scaffolds promote angiogenesis, preserve heart function, and reduce left ventricular remodeling in rat acute myocardial infarction. Am J Transl Res **7,** 781, 2015.
43. Huang, H., Liu, J., Hao, H., *et al.* Preferred M2 polarization by ASC-based hydrogel accelerated angiogenesis and myogenesis in volumetric muscle loss rats. Stem Cells Int **2017,** 2896874, 2017.
44. Kachgal, S., and Putnam, A.J. Mesenchymal stem cells from adipose and bone marrow promote angiogenesis via distinct cytokine and protease expression mechanisms. Angiogenesis **14,** 47, 2011.
45. Liang, X., Zhang, L., Wang, S., Han, Q., and Zhao, R.C. Exosomes secreted by mesenchymal stem cells promote endothelial cell angiogenesis by transferring miR-125a. J Cell Sci **129,** 2182, 2016.
46. Pinheiro, C.H., de Queiroz, J.C., Guimarães-Ferreira, L., *et al.* Local injections of adipose-derived mesenchymal stem cells modulate inflammation and increase angiogenesis ameliorating the dystrophic phenotype in dystrophin-deficient skeletal muscle. Stem Cell Rev **8,** 363, 2012.
47. Seo, E., Lim, J.S., Jun, J.B., Choi, W., Hong, I.S., and Jun, H.S. Exendin-4 in combination with adipose-derived stem cells promotes angiogenesis and improves diabetic wound healing. J Transl Med **15,** 35, 2017.
48. Rehman, J., Traktuev, D., Li, J., *et al.* Secretion of angiogenic and antiapoptotic factors by human adipose stromal cells. Circulation **109,** 1292, 2004.
49. Trouillet, A., Lorach, H., Dubus, E., *et al.* Col4a1 mutation generates vascular abnormalities correlated with neuronal damage in a mouse model of HANAC syndrome. Neurobiol Dis **100,** 52, 2017.
50. Yang, W., Ng, F.L., Chan, K., *et al.* Coronary-heart-disease-associated genetic variant at the COL4A1/COL4A2 locus affects COL4A1/COL4A2 expression, vascular cell survival, atherosclerotic plaque stability and risk of myocardial infarction. PLoS Genet **12,** e1006127, 2016.
51. Alavi, M.V., Mao, M., Pawlikowski, B.T., *et al.* Col4a1 mutations cause progressive retinal neovascular defects and retinopathy. Sci Rep **6,** 18602, 2016.
52. Van Agtmael, T., Bailey, M.A., Schlötzer-Schrehardt, U., *et al.* Col4a1 mutation in mice causes defects in vascular function and low blood pressure associated with reduced red blood cell volume. Hum Mol Genet **19,** 1119, 2010.
53. Frank, M., Albuisson, J., Ranque, B., *et al.* The type of variants at the COL3A1 gene associates with the phenotype and severity of vascular Ehlers–Danlos syndrome. Eur J Hum Genet **23,** 1657, 2015.
54. Yan, H., Zhang, C., Wang, Z., *et al.* CD146 is required for VEGF-C-induced lymphatic sprouting during lymphangiogenesis. Sci Rep **7,** 7442, 2017.
55. Chen, J., Luo, Y., Hui, H., *et al.* CD146 coordinates brain endothelial cell-pericyte communication for blood–brain barrier development. Proc Natl Acad Sci U S A **114,** E7622, 2017.
56. Kebir, A., Harhouri, K., Guillet, B., *et al.* CD146 short isoform increases the proangiogenic potential of endothelial progenitor cells in vitro and in vivo. Circ Res **107,** 66, 2010.
57. Harhouri, K., Kebir, A., Guillet, B., *et al.* Soluble CD146 displays angiogenic properties and promotes neovascularization in experimental hind-limb ischemia. Blood **115,** 3843, 2010.
58. Nandadasa, S., Nelson, C.M., and Apte, S.S. ADAMTS9-mediated extracellular matrix dynamics regulates umbilical cord vascular smooth muscle differentiation and rotation. Cell Rep **11,** 1519, 2015.
59. Koo, B.H., Coe, D.M., Dixon, L.J., *et al.* ADAMTS9 is a cell-autonomously acting, anti-angiogenic metalloprotease expressed by microvascular endothelial cells. Am J Pathol **176,** 1494, 2010.
60. Rojas-Rodriguez, R., Gealekman, O., Kruse, M.E., *et al.* Adipose tissue angiogenesis assay. Methods Enzymol **537,** 75, 2014.
61. Chung, M.T., Hyun, J.S., Lo, D.D., *et al.* Micro-computed tomography evaluation of human fat grafts in nude mice. Tissue Eng C Methods **19,** 227, 2013.
62. Chen, J., Bardes, E.E., Aronow, B.J., and Jegga, A.G. ToppGene Suite for gene list enrichment analysis and candidate gene prioritization. Nucleic Acids Res **37,** W305, 2009.
63. Schindelin, J., Arganda-Carreras, I., Frise, E., *et al.* Fiji: an open-source platform for biological-image analysis. Nat methods **9,** 676, 2012.

Address correspondence to:
Silvia Corvera, MD
Program in Molecular Medicine
University of Massachusetts Medical School
373 Plantation Street
Worcester, MA 01605

E-mail: silvia.corvera@umassmed.edu

Received: February 26, 2018
Accepted: July 3, 2018
Online Publication Date: January 2, 2019